

Multiple generation in normal incidence synthetic seismograms

Chanpen Silawongsawat and Gary F. Margrave

ABSTRACT

An elastic modeling algorithm for a 2D stratified medium is introduced. The technique uses phase shift extrapolation in depth for wavefield propagation and the explicit Zoeppritz equations for reflection, transmission and mode conversion. All possible multiples and mode conversions may be computed by cascading each horizontal wavenumber through a computation grid similar to that used in 1D seismograms.

As an initial test, we have implemented the algorithm in the 1D acoustic case and compared its results to the conventional technique (time domain method). The time domain method is so named because it resamples the depth model into layers of equal traveltime. Since our method does not resample the model, we expect its results to be more theoretically correct. We used four synthetic models, two of a constant velocity and two of a constant density, from two typical impedance cases: step model and random model. Our algorithm and the time domain algorithm are equivalent for constant velocity but can give quite different results in other cases. For variable velocity models our algorithm generates results which meet theoretical expectations for both primaries and multiples but which differ in details from results of the time domain method. We also compared the two methods on real Blackfoot 08-08 well log data. Both algorithms produce a series of spectral notches due to the effects of the Mannville coals though the seismograms themselves are very different.

INTRODUCTION

We present an elastic modeling algorithm which uses the Gazdag phase shift method (Gazdag, 1978) to extrapolate P and SV (hereafter just S) vertically (in z) through a layered medium. The Zoeppritz equations are used for reflectivity calculations. Features of the method include:

- An arbitrary number of layers with arbitrary thicknesses and elastic parameters (v_p , v_s , and ρ).
- Each k_x wavenumber is handled completely independently (though it may always be possible to deduce negative from positive wavenumbers by symmetry).
- Four independent wavefields are maintained: downgoing and upgoing P and downgoing and upgoing S.
- Coupling between the wavefields occurs at each interface (or Δz step) using the exact Zoeppritz equations.
- Extrapolation across a layer is done with the Gazdag phase shift method ($f-k_x$) and is thus highly accurate. Rather than abruptly rejecting evanescent energy, it is subjected to exponential decay, which allows waves to “leak” across thin high velocity layers which they could not penetrate with ray theory.

- All possible mode conversions and multiples can be generated or various effects can be turned off to generate “primaries only” or “P only” or similar options. The methodology for doing this is an extension of 1D vertical seismogram methods such as that of Waters (1992).

Most elastic wave modeling formulations amount to a direct simulation of the elastic wave equations using either finite difference (Kelly et al., 1976), finite element (Kennett, 1980, Fuchs and Müller, 1971), or spectral methods. Hence these methods do not formally use results like the Zoeppritz equations since they are implicitly contained in the elastic wave equations. Though they produce very realistic results, elastic wave methods are not popular because the results tend to be as difficult to interpret as real data and the algorithms do not typically allow effects to be turned on and off. Ray trace elastic methods, like SYNTH (Lawton and Howell, 1992, Margrave and Foltinek, 1995), use Snell's law for ray paths and the Zoeppritz equations for amplitudes. As such, they are much more flexible than full elastic wave methods but tend to lack realism in ways that are mostly attributable to the raytracing. The method proposed here falls between these two approaches. Phase shift extrapolation replaces Snell's law raytracing but the Zoeppritz equations are still used explicitly. The result should be greater realism than SYNTH but more flexibility than traditional elastic wave modeling. A method similar in intent to the one proposed here but limited to non-evanescent plane waves and equal traveltimes layers can be found in Easley and Foltinek (1993).

To test these concepts, we have implemented our algorithm in the 1D acoustic case and compare it with the method commonly used in the exploration industry (Berryman et al., 1958, Waters, 1992, Easley and Foltinek, 1993, Hubral et al., 1980). We will refer to our technique as the depth domain method and to the industry technique as the time domain method (it is also often called the Goupillaud seismogram). The phrase “time domain” refers to the fact that the standard method requires the input model to have layer thicknesses chosen such that the two-way traveltimes across all the layers is constant. Usually the constant traveltimes is taken to be the desired time sample rate of the output seismogram and the input model is taken from well logs which will be resampled to have constant layer traveltimes. Originally, this resampling was done to reduce computational times but theoretical justification for it is lacking. Our method does not involve such a resampling, though like the time domain method, it can still compute all possible multiples. A major effect of the equal traveltimes resampling is a strong smoothing of the well log reflectivity. This can be appreciated by considering that logs are usually sampled at about 1/3 meter intervals and supposing a typical velocity of 3000 m/s we see that roughly ten depth samples are averaged to obtain .002 second layers. This averaging can be expected to alter the character of the seismogram and we will investigate this effect.

THEORY

The Gazdag extrapolation of P waves can be written as:

$$\phi(k_x, z + \Delta z, \omega) = \phi(k_x, z, \omega) \exp \left(i \Delta z \sqrt{\frac{\omega^2}{v_p^2(z)} - k_x^2} \right) \quad (1)$$

where $\phi(k_x, z, \omega)$ is the wavefield in (k_x, ω) space at depth z , v_p is the P wave velocity, and Δz is the extrapolation step size. This complex exponential form is easily derived from the scalar wave equation and the sign of Δz determines whether the extrapolation

is up (negative z direction) or down. (We will assume that a positive Δz results in downward extrapolation.) This extrapolation formalism is highly accurate (no grid dispersion, steep dips well handled if not aliased, etc.) and contains all "geometric" propagation effects. The latter means that it correctly computes the spatial position of waves in a $v(z)$ medium and applies spherical divergence. To extrapolate S waves, it is only necessary to use v_s in place of v_p .

If we wish to adapt this expression to include a transmission loss factor, it is easy to do so as:

$$\phi(k_x, z + \Delta z, \omega) = \phi(k_x, z, \omega) T_{pp}(\theta, z) \exp\left(i\Delta z \sqrt{\frac{\omega^2}{v_p^2(z)} - k_x^2}\right) \quad (2)$$

Here T_{pp} symbolizes the appropriate transmission coefficient for P waves incident from above a horizontal interface as given by the Zoeppritz equations (Aki and Richards, 1980). Note that since the Fourier transform is essentially a plane wave decomposition, this expression is actually the appropriate way to apply the Zoeppritz equations which are derived explicitly for plane wave incidence. T_{pp} is purely a function of wave incidence angle, θ , and depth for known elastic material parameters.

If we wish to convert P to S on transmission, we would use a similar expression with T_{ps} in place of T_{pp} . Reflections, with or without mode conversions, are handled in like manner. The Zoeppritz transmission and reflection coefficients depend on material parameters on both sides of the interface and on the incident angle. The material parameters are presumed known and the incident angle is given by:

$$\sin(\theta(z)) = \frac{v(z)k_x}{\omega} \quad (3)$$

where $v(z)$ denotes the velocity appropriate for the incident wave. Thus we see that the appropriate coefficient is simply a function of the model and the spectral coordinates (k_x, ω) .

Now consider the implications of Snell's law in this scheme. Since a radial line in (k_x, ω) space is a line of constant horizontal slowness (this follows directly from (3)), and since Snell's law for a $v(z)$ medium says simply to conserve horizontal slowness (even for converted waves), we conclude that spectral components in (k_x, ω) do not "move around" but are simply scaled and phase shifted as a wave propagates and converts modes. Thus the (k_x, ω) transform is a very appropriate method for this purpose.

A further point to consider is the behavior of (1) for $k_x^2 > \frac{\omega^2}{v^2(z)}$. In this case the square root in the exponential becomes imaginary and the exponential changes from a complex sinusoid to a growing or decaying (both are mathematically allowed) real exponential. In ray theory, this corresponds to incidence beyond the critical angle whereas in wavefield extrapolation jargon it is customary to use this inequality to divide the spectrum into wavelike and evanescent regions. Usually the evanescent energy is simply zeroed because it decays with an exponential decay constant of roughly the vertical wavelength. That is, after several wavelengths the energy is quite highly

attenuated and (1) is usually used in migration algorithms where step sizes can be quite large. However, for elastic modeling, it is better to allow the exponential decay to proceed as mathematically expected (exponential growth is rejected on physical grounds). This has the effect of stabilizing the model in the presence of thin high velocity layers as are commonly found in well logs. At such a layer, this method will consider a portion of the spectrum to be evanescent but the decay distance will be a small fraction of a wavelength and the wave will cross the layer. (This is the direct analog of quantum mechanical tunneling.)

ALGORITHM

Let:

$\phi_{pd}(z)$ denote the downgoing P wave at depth z and spectral coordinates (k_x, ω) .

$\phi_{pu}(z)$ denote the upgoing P wave at depth z and spectral coordinates (k_x, ω) .

$\phi_{sd}(z)$ denote the downgoing S wave at depth z and spectral coordinates (k_x, ω) .

$\phi_{su}(z)$ denote the upgoing S wave at depth z and spectral coordinates (k_x, ω) .

Given these four wavefields, the computation of the elastic seismogram can be done, for fixed k_x , in a manner quite similar to the established theory for a 1D normal incidence seismogram (Waters, 1992). The most obvious difference is that at each computation node there are four incident and four resultant wavefields (instead of two and two). In the 1D case it was sufficient to represent the propagating wave as a single impulse which gets scaled by reflection and transmission coefficients. In the current situation, a vector of ω 's must be propagated for each k_x because the evanescent effect causes bandwidth alterations in the wavefield which must be recorded. At each node, the four wavefields can be related by a "scattering matrix" (Aki and Richards 1980) with elements which are found from the Zoeppritz equations:

$$\begin{bmatrix} \bar{\phi}_{pd} \\ \bar{\phi}_{pu} \\ \bar{\phi}_{sd} \\ \bar{\phi}_{su} \end{bmatrix} = \begin{bmatrix} T_{pp} & R_{pp}^- & T_{sp} & R_{sp}^- \\ R_{pp} & T_{pp}^- & R_{sp} & T_{sp}^- \\ T_{ps} & R_{ps}^- & T_{ss} & R_{ss}^- \\ R_{ps} & T_{ps}^- & R_{ss} & T_{ss}^- \end{bmatrix} \begin{bmatrix} \phi_{pd} \\ \phi_{pu} \\ \phi_{sd} \\ \phi_{su} \end{bmatrix} \quad (4)$$

Here the - superscripts on the reflection or transmission coefficients indicate the form for the incident wave from beneath is used. The waves on the left are the resultant (scattered) waves and are distinguished with an upper bar. Since the wavefields in (4) are vectors of ω 's, we apply (4) for each ω .

Figure 1 shows the computation grid. (The layers are depicted of equal thickness for graphical simplicity but there is no such requirement in the algorithm. In fact, it will probably be desirable to have a large initial layer to represent an overburden above a logged interval.) Beginning at step 1, layer 1, the four wavefields are initialized as prescribed by the source. (For surface sources the upgoing waves will be zero, for buried sources we can start at step 2 layer 2.) Assuming that we have only two downgoing waves at this point, we extrapolate them to layer 2 with equation (1) using v_p and v_s as appropriate. Then applying (4), we compute the four scattered waves. The upgoing waves are then upward extrapolated and the downgoing waves are downward

extrapolated so that we have the inputs to each of the 2 nodes at step 3. Applying (4) to each node, the process continues until the reflected waves from the deepest reflector have been propagated back up to the surface. It is evident that at the j th step in the algorithm, there are $(j+1)/2$ active nodes in the diagram for which we must maintain wavefields in computer memory.

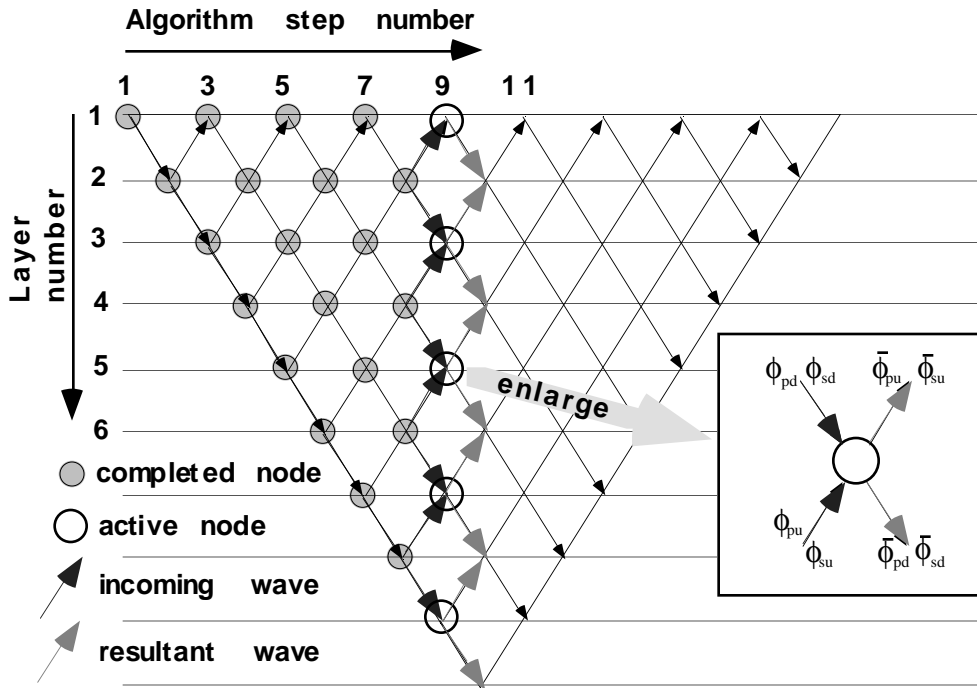


Fig 1. The computation grid for the 1.5D elastic seismogram. Each k_x component is propagated independently through the grid. The total number of algorithmic steps is $2*nz-1$ where nz is the number of layers. At the j th step, simultaneous wavefields must be held in memory for $(j+1)/2$ nodes. Each node has four incident and four resultant wavefields which are related via the scattering matrix. The algorithm is at step 9 of 19 in the diagram.

The calculation requires maintaining four arrays in memory for each of the propagating wavefields and two more arrays for accumulating the P and S waves at $z=0$. Each propagating wavefield array contains one column of ω 's for each active node at any given step in the algorithm. As the calculation progresses from step 1 to step nz , the propagating wavefield arrays grow to a maximum size and then decrease until step $2*nz-1$.

The scattering matrix can be altered to turn off various effects. For example, to compute a primaries only seismogram, we set to zero all scattering terms which convert modes on transmission or which reflect from the bottom of an interface:

$$\begin{bmatrix} \bar{\phi}_{pd} \\ \bar{\phi}_{pu} \\ \bar{\phi}_{sd} \\ \bar{\phi}_{su} \end{bmatrix} = \begin{bmatrix} T_{pp} & 0 & 0 & 0 \\ R_{pp} & T_{pp}^- & R_{sp} & 0 \\ 0 & 0 & T_{ss} & 0 \\ R_{ps} & 0 & R_{ss} & T_{ss}^- \end{bmatrix} \begin{bmatrix} \phi_{pd} \\ \phi_{pu} \\ \phi_{sd} \\ \phi_{su} \end{bmatrix} \quad (5)$$

Similar considerations can be used to create "P waves only", "converted waves only" and so on.

The proposed algorithm can be summarized in pseudo-code as:

- initialize the model
- determine source waveform
- for each k_x
 - initialize the source wavefields
 - for each Δz step
 - for each active node
 - propagate (Gazdag phase shift) the four wavefields up and down to the next nodes
 - compute the four scattered wavefields with the scattering matrix
 - end
 - sum any waves arriving at a surface node into the output arrays for P and S with appropriate free surface corrections (Dankbaar 1995)
 - end
- end
- resolve accumulated P and S wavefields at $z=0$ into horizontal and vertical displacement components.

Reduction to 1D is quite simple and conceptually amounts to running the k_x loop only once for $k_x = 0$. Additional simplifications are that only two wavefields must be computed at each node and the Zoeppritz reflection and transmission coefficients become the simple normal incidence expressions.

APPLICATION AND RESULTS

Primaries-plus-multiples synthetic seismograms created by the time domain method often are difficult to match to seismic data while primaries-only synthetics usually tie well. This may be due in part to the fact that seismic processing is designed to attenuate multiples but it may also indicate a problem with multiple generation in synthetic seismograms. Therefore we want to examine multiple generation by our depth domain algorithm compared to the time domain algorithm. We consider two simple acoustic impedance situations whose effects have been described by O'Doherty and Anstey(1971) and Waters(1992). These are monotonic changes in impedance and alternating impedance changes (Figure 2). They are the two end members of a possible continuum of models which cause interbed multiples (O'Doherty and Anstey, 1971). We call them the step impedance model and the random impedance model respectively.

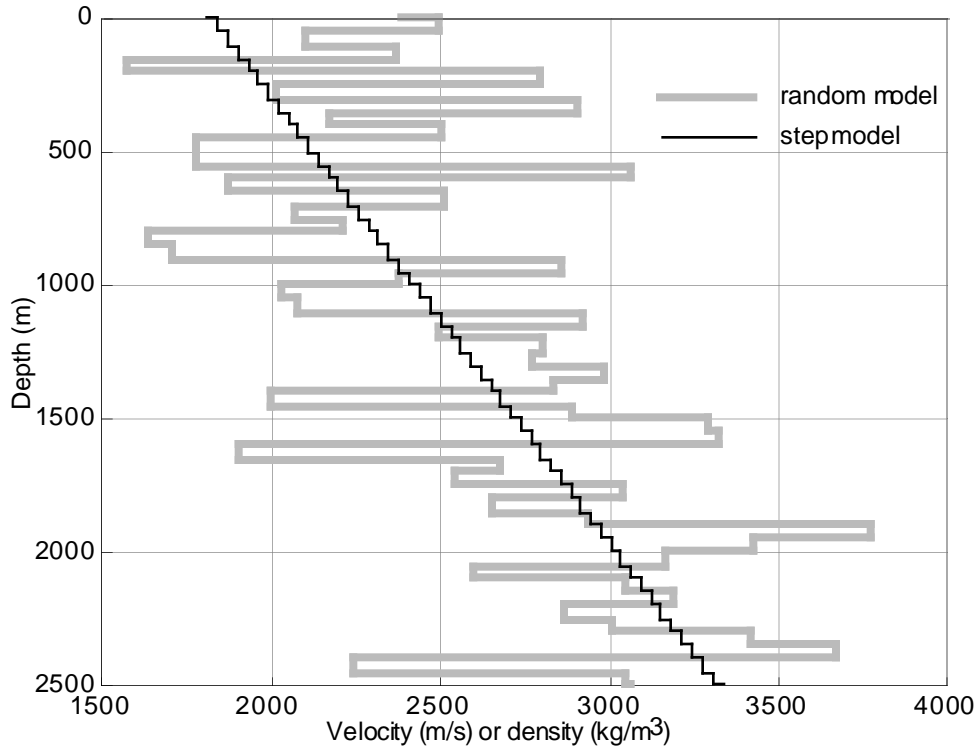


Fig. 2. Synthetic acoustic impedance models The curved give either density for the constant velocity model or velocity for the constant density model. The constant velocity or density is 2500 (in MKS units)

We show two versions of each model where the impedance is the same in each version but in one case the density is held constant at 2500 kg/m^3 and in the other case velocity is kept constant at 2500 m/s . The step model shows the impedance increasing at each depth interval (according to $\text{Imp}=2500*(1800+0.6*Z)$) while the random model has impedance fluctuations about the same trend.

For the step model, the generated first-order multiples are opposite in sign to the primary pulses. Though each multiple must be small, the total effect can become very large through the superposition of events from many layers. Since the primaries are steadily decreasing through transmission losses, the multiples will eventually dominate and could cause an apparent flip of polarity (Waters, 1992)

The random model produces large reflection coefficients of alternating signs. Most of the first-order multiples generated by this model are relatively large and of the same polarity as the primaries. With enough layers, the amplitude of the composited multiples can surpass that of the primaries (Waters, 1992).

Our purpose in assuming constant velocity in the two impedance cases is to force all of the reflection coefficients to be exactly at output sample times. The depth interval for each layer is 50 meters and with constant velocity of 2500 m/s the time thickness of every layer will be 40 ms which will fall precisely on output sample times for the sample rate we use (2 ms). Therefore the time domain algorithm does not need to resample the model and the results from both methods should be identical. The constant density models were chosen as a contrast to the constant velocity case. We expect the differences between the two methods will be very obvious in this case. Since the layer

traveltime now fluctuates, the time domain algorithm must alter the depth layering considerably.

Thus we examine four synthetic acoustic impedance models : (1) step model with constant density, (2) random model with constant density, (3) step model with constant velocity and (4) random model with constant velocity. In addition, we also show real data results from the Blackfoot 08-08 well log data. The density and velocity logs from Blackfoot 08-08 are shown in Figure 3. The Mannville coals, which are a known source of multiple problems are located between 1500-1750m.

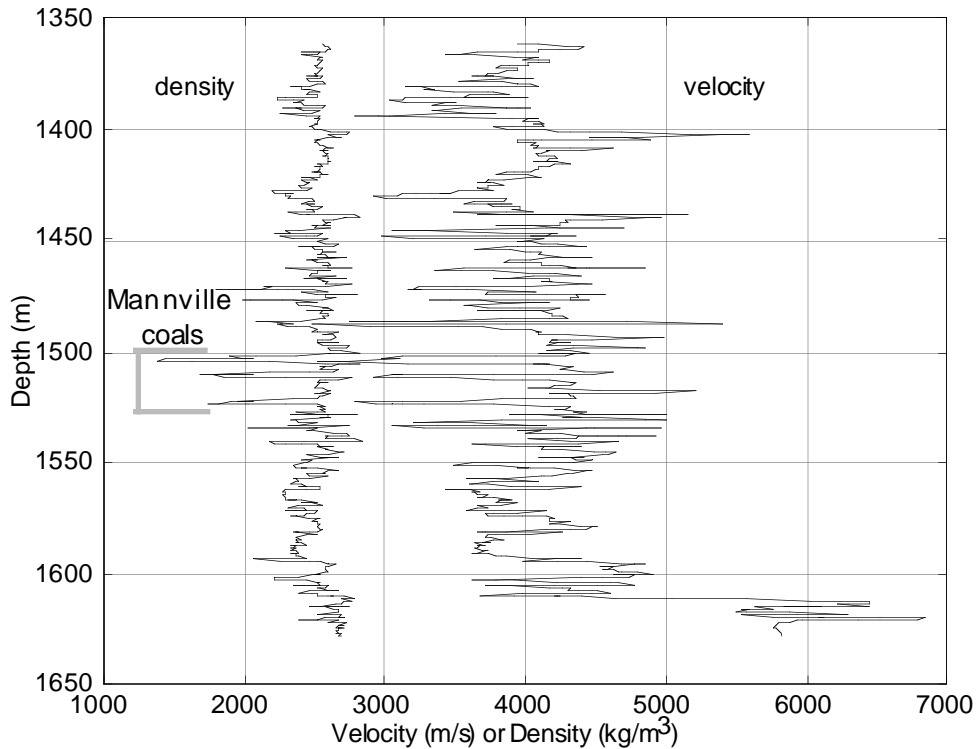
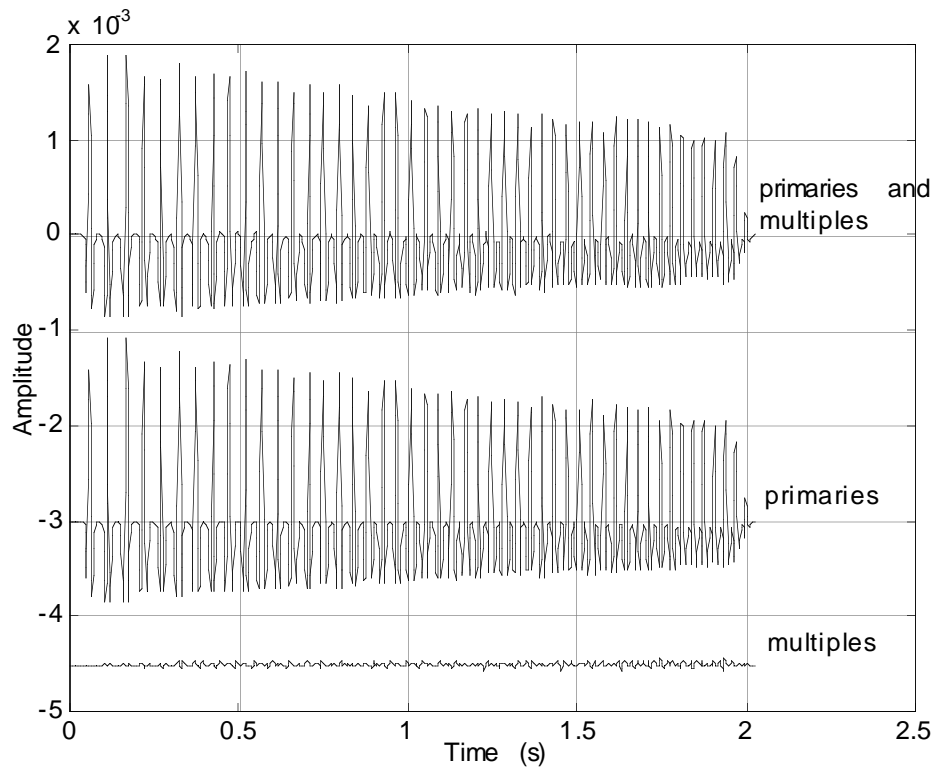


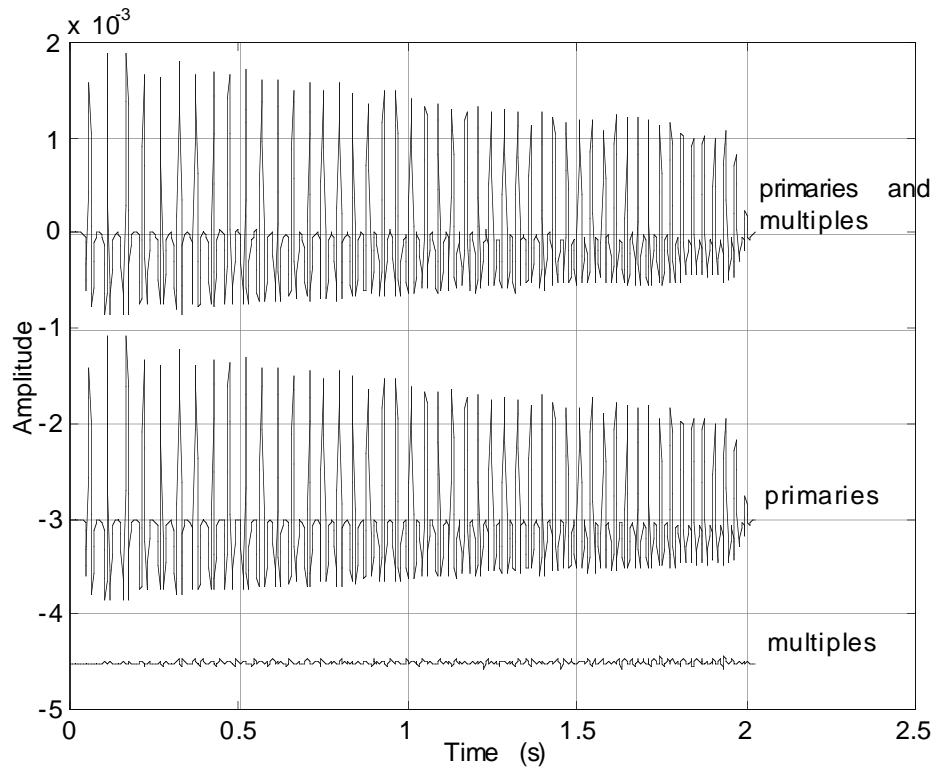
Fig. 3. Interval velocity and density of Blackfoot 08-08 well logs

Figures 4, 6, 8 and 10 display responses of both algorithms to each artificial model. They are all band limited with a 50Hz Ricker wavelet to make the physical effects more apparent. At first glance, the differences between the two methods are difficult to distinguish. The 50m layer thickness of these models are much larger than real well logs. We expect that smaller layers will give more obvious differences as we show with our real data example. To aid in the comparison, Figures 5, 7, 9 and 11 are difference plots of primaries and multiples for each case.

Considering the step model, as we expected, the primaries are all positive, multiples are negative and both are relatively small (Figures 4 and 6). From the comparison in Figure 5, there are slight differences of primaries and multiples between the time domain and depth domain solutions. On the other hand, for the constant velocity results in Figure 7 primaries and multiples produced by time domain and depth domain calculations are exactly alike and more mathematically regular than in the constant density case. Notice that primaries and multiples in Figure 7 appear evenly along time axis while in Figure 5 only the primaries show systematic spacing. The multiples in Figure 5 are initially regular but then become chaotic.

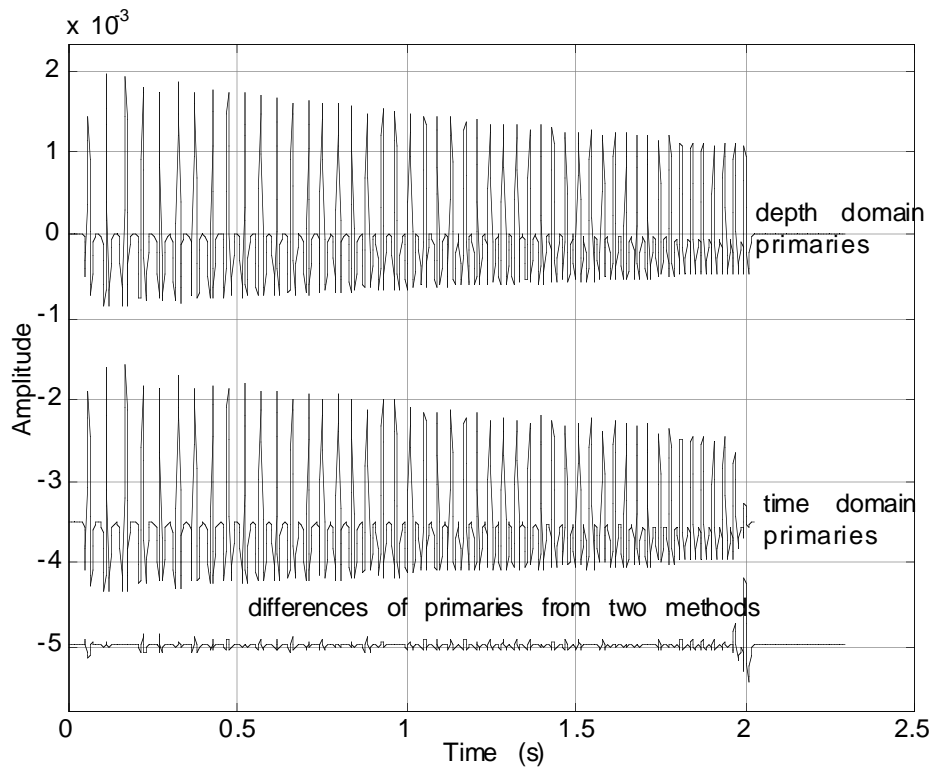


(a) Depth domain method

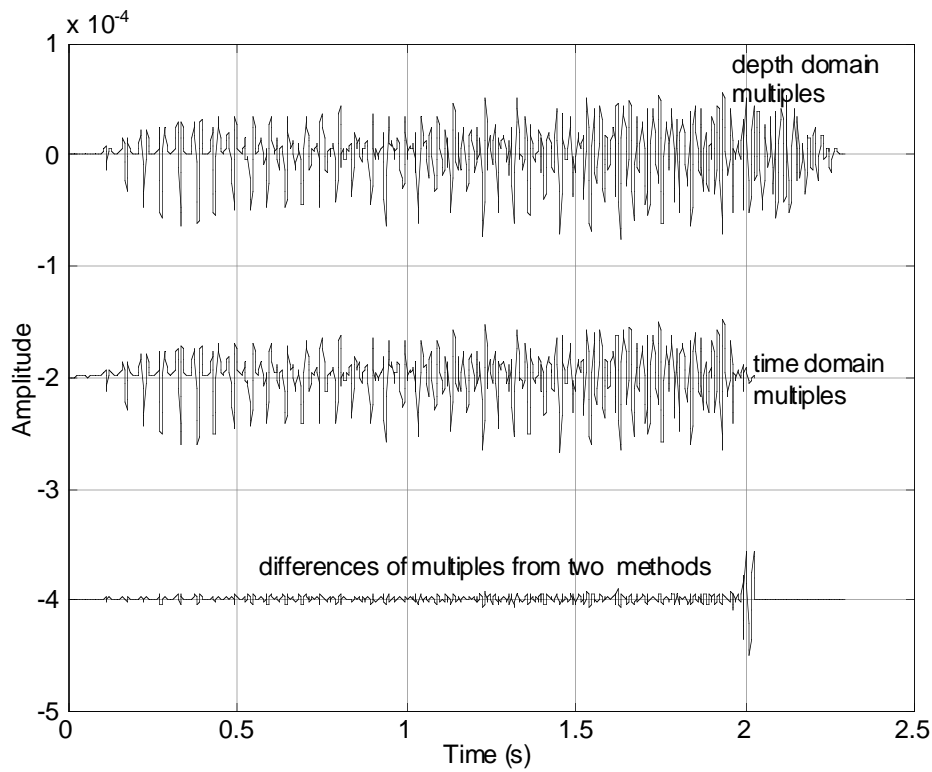


(b) Time domain method

Fig. 4. Responses of the two methods for the constant density step model

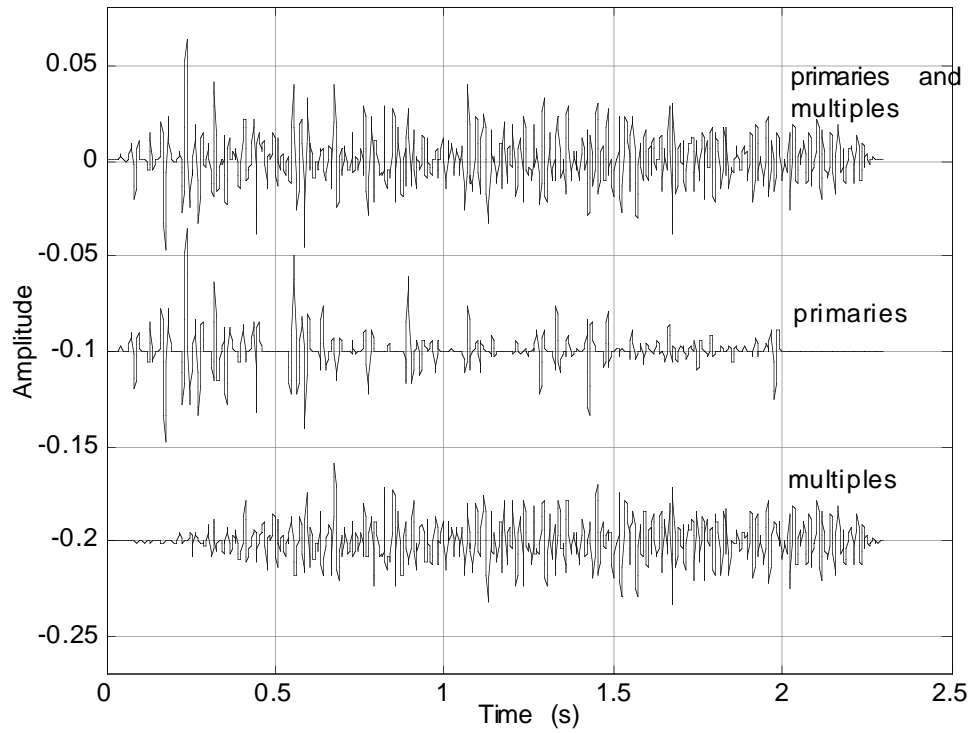


(a) Primaries

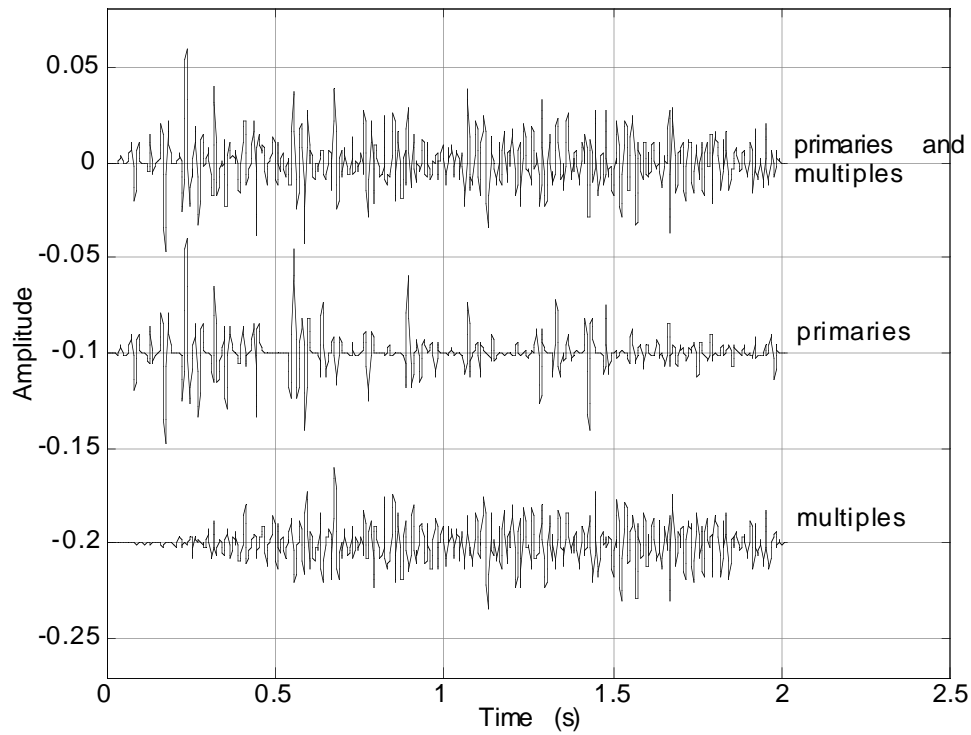


(b) Multiples

Fig. 5. Comparisons with difference plots for constant density step model.

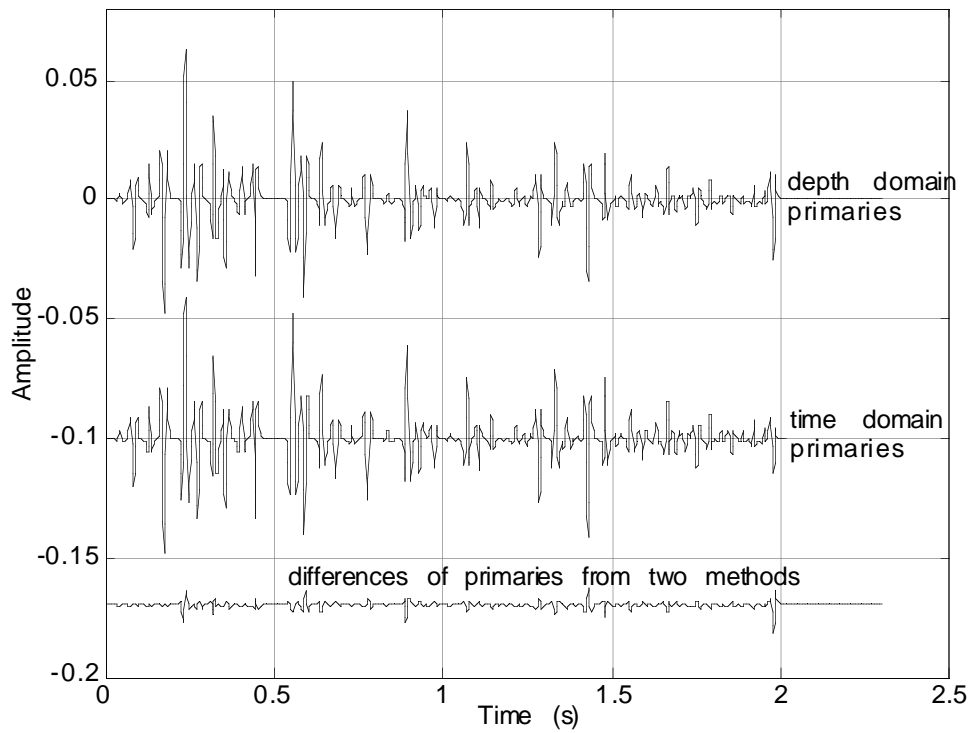


(a) Depth domain method

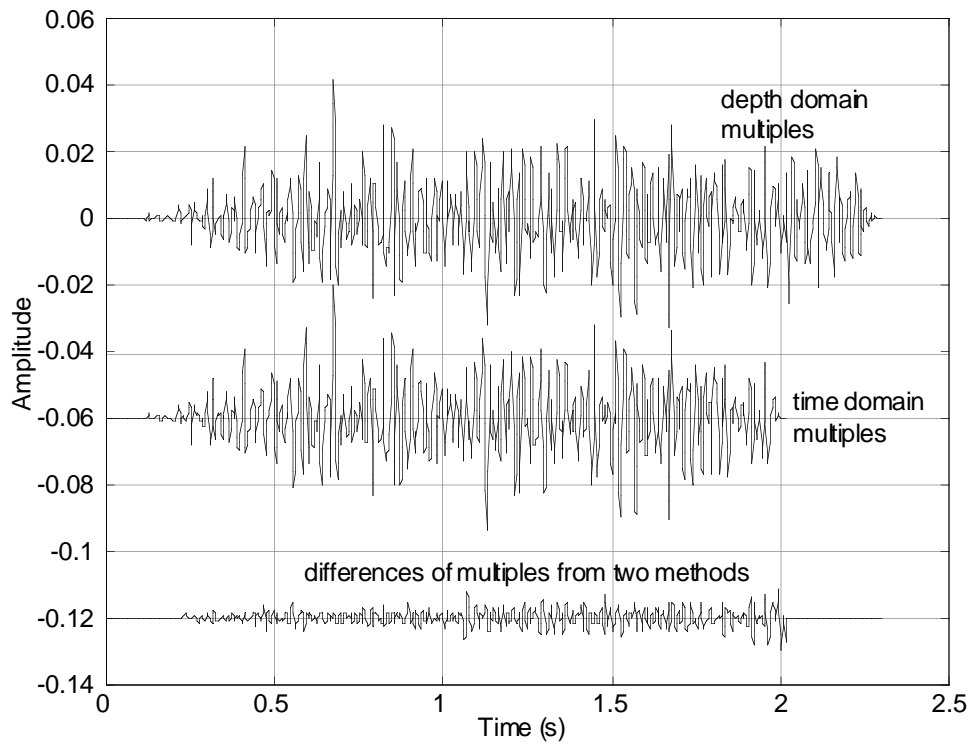


(b) Time domain method

Fig. 6. Responses of the two methods for the constant density random model

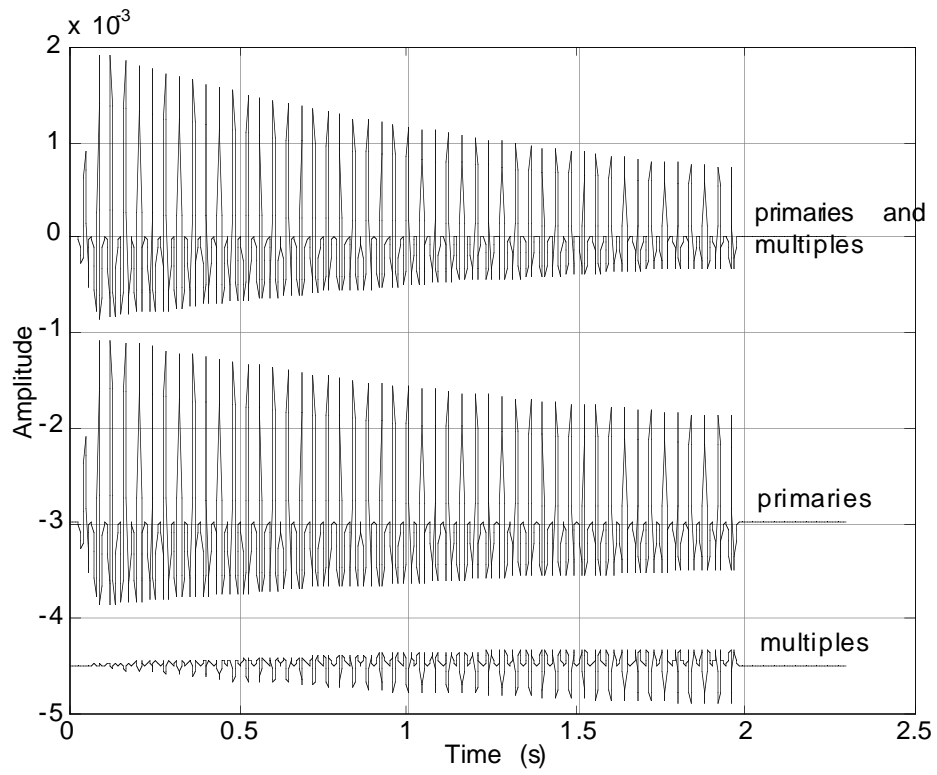


(a) Primaries

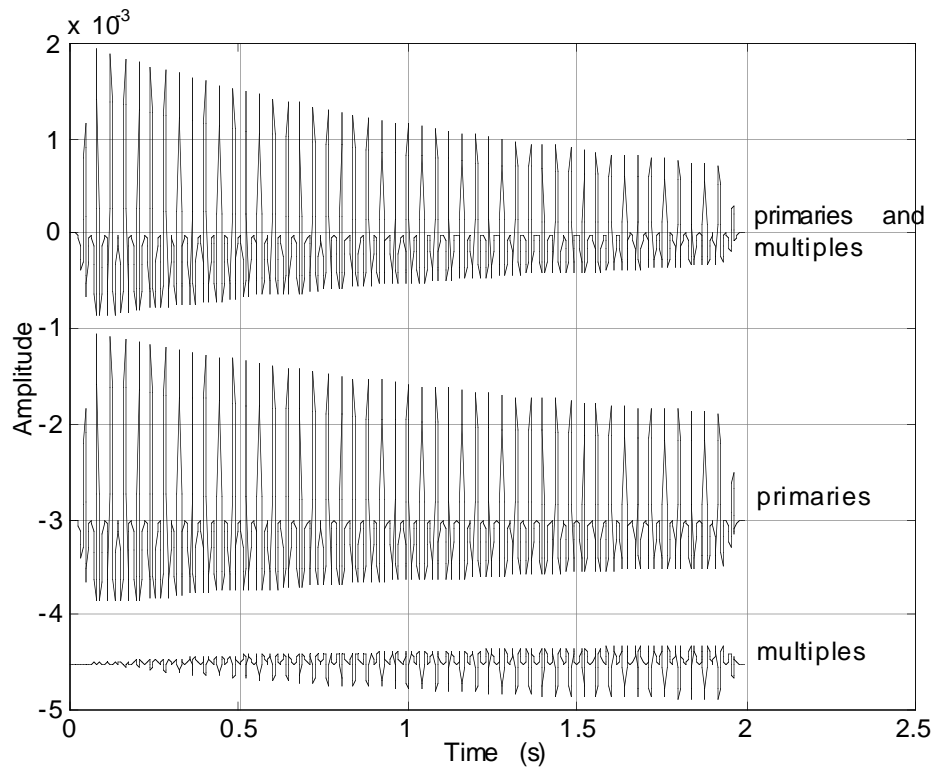


(b) Multiples

Fig. 7. Comparisons with difference plots for the constant density random model.

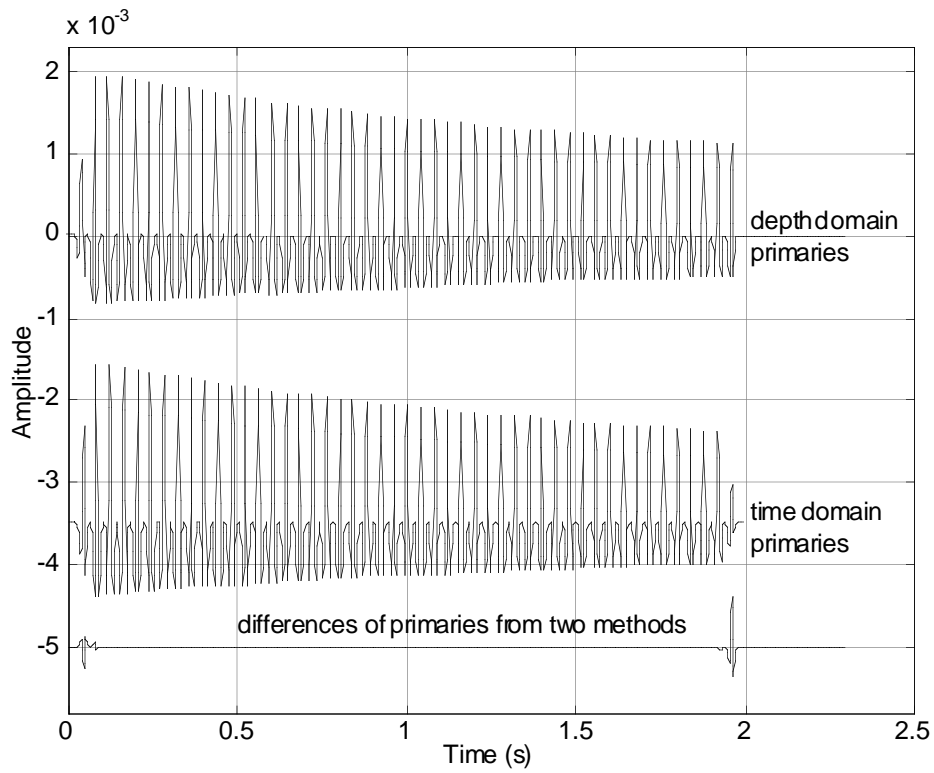


(a) Depth domain method

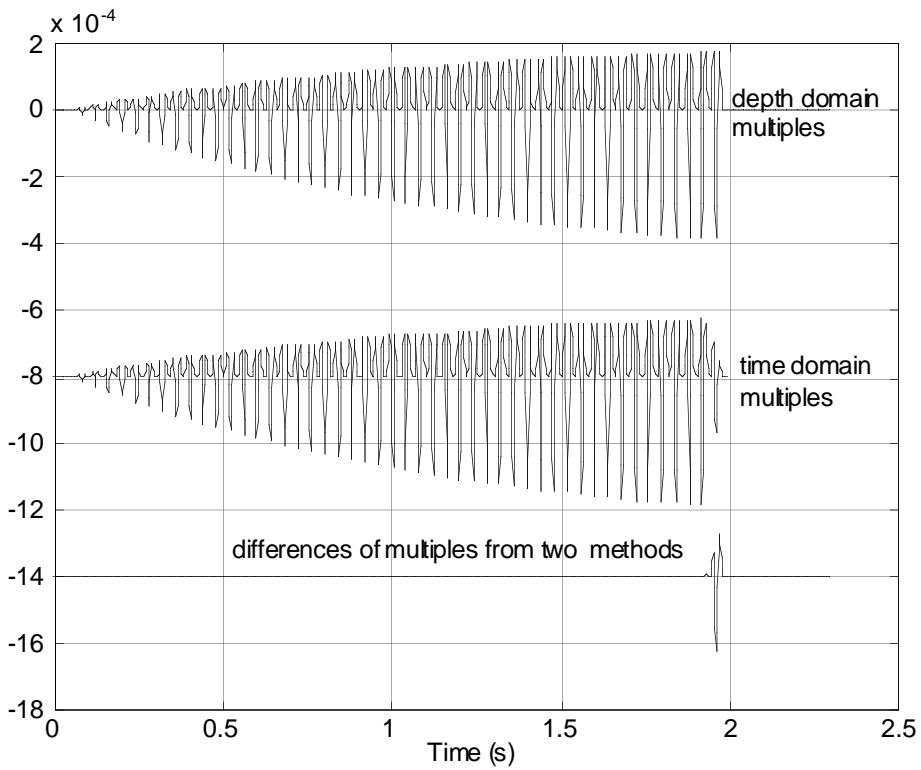


(b) Time domain method

Fig. 8. Responses of the two methods for the constant velocity step model

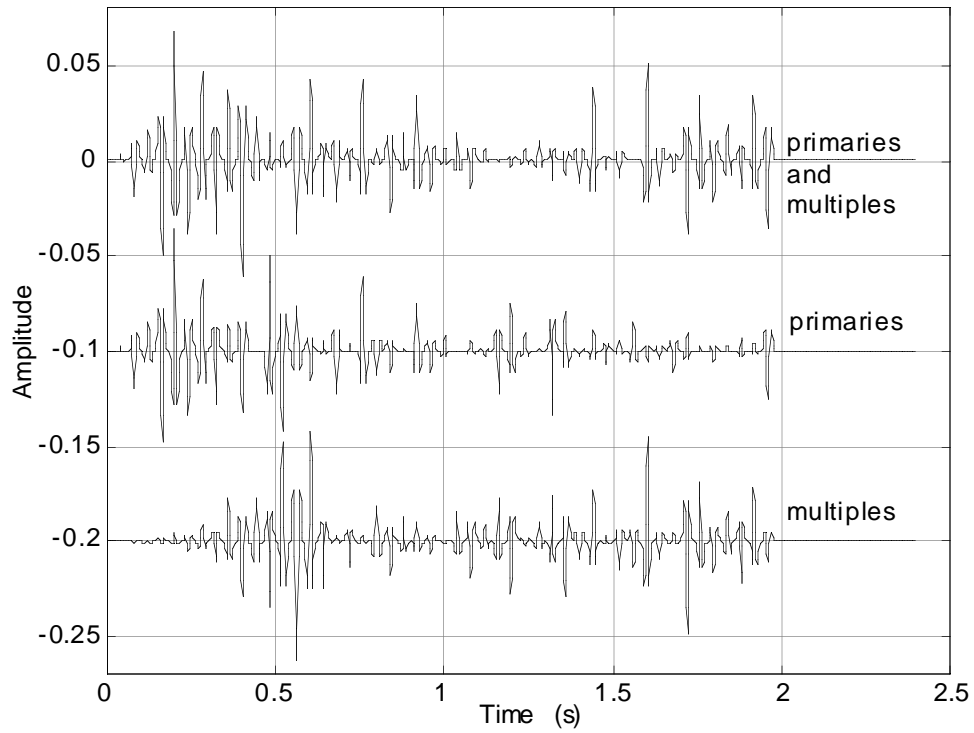


(a) Primaries

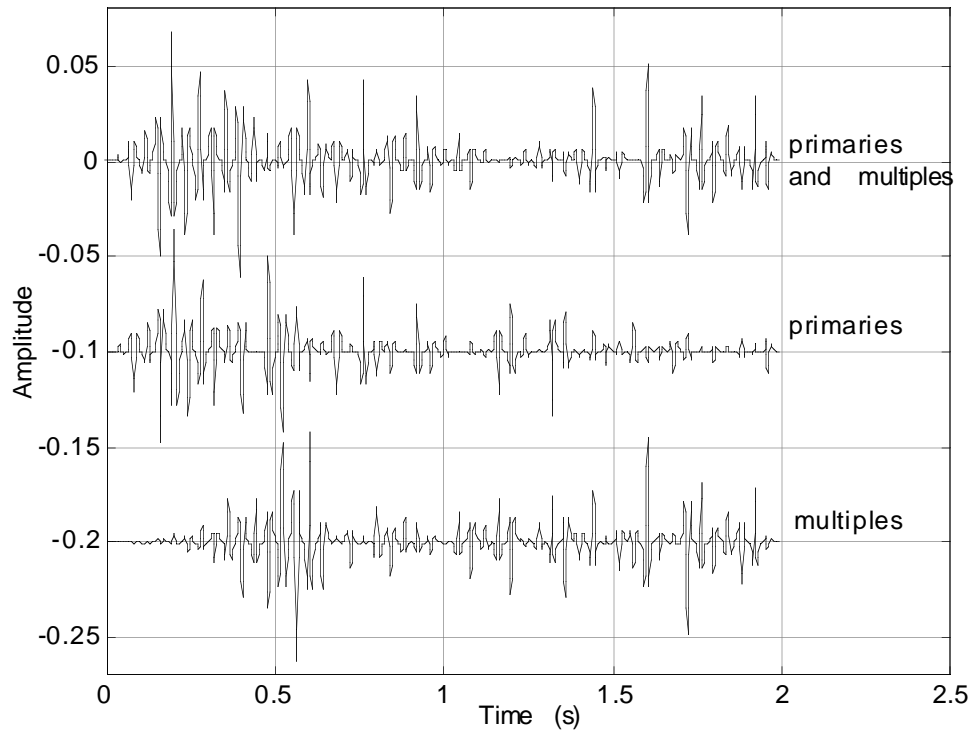


(b) Multiples

Fig. 9. Comparisons with difference plots for the constant velocity step model.

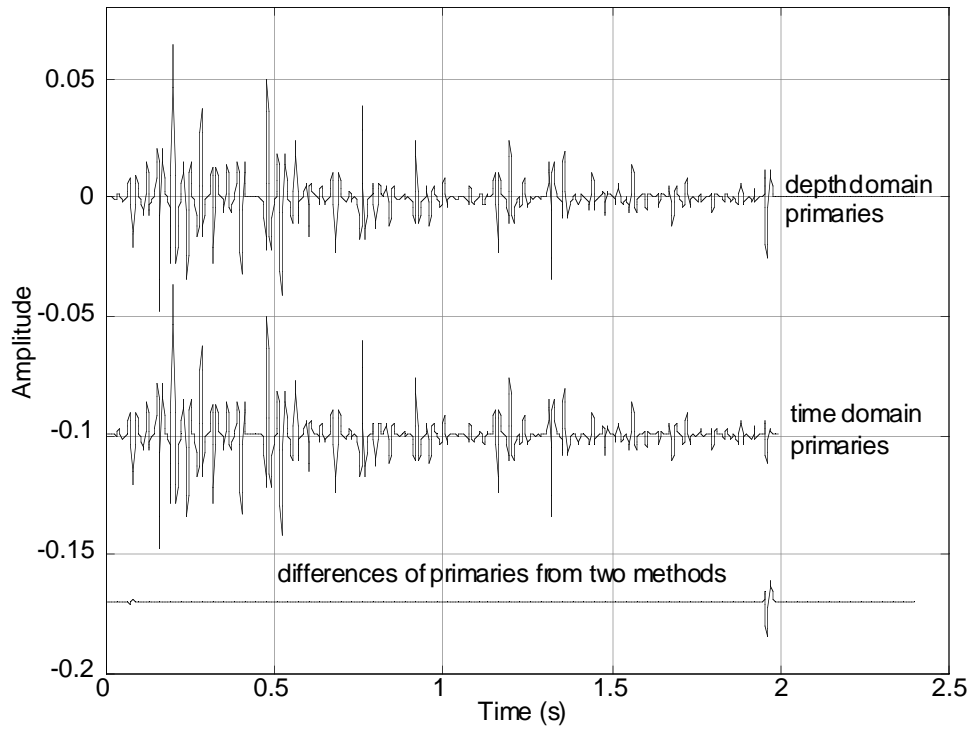


(a) Depth domain method

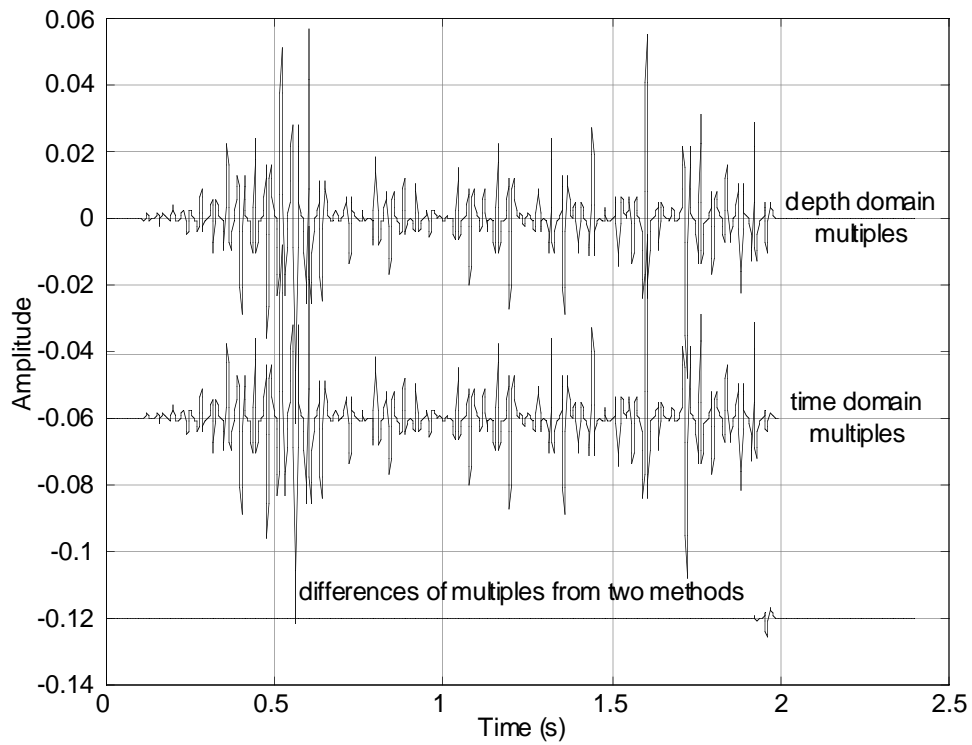


(b) Time domain method

Fig. 10. Responses of the two methods for the constant density random model

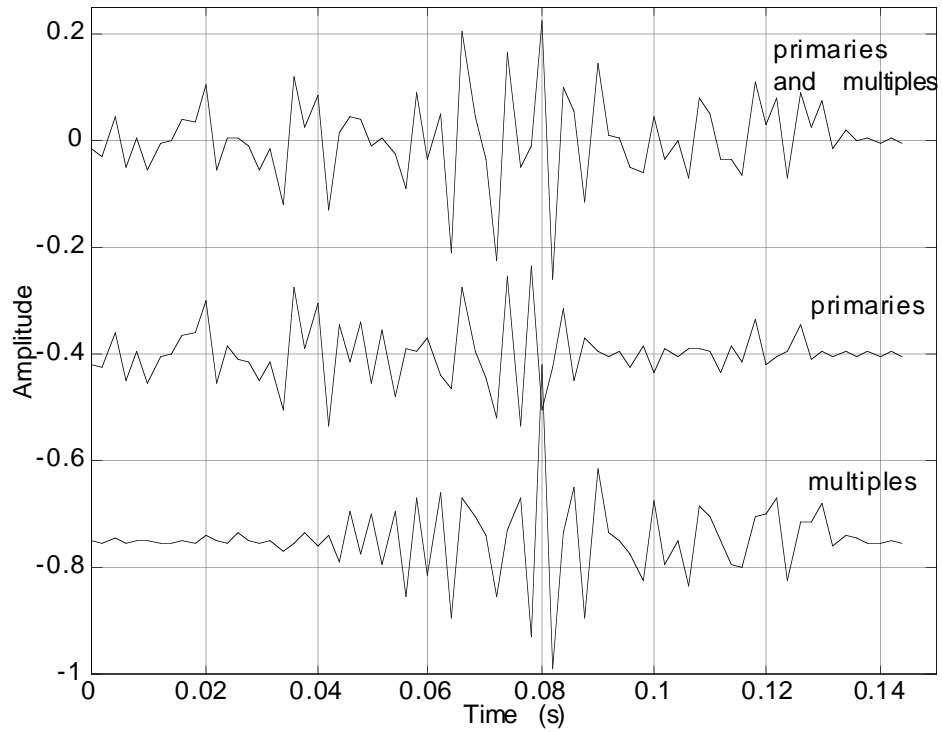


(a) Primaries

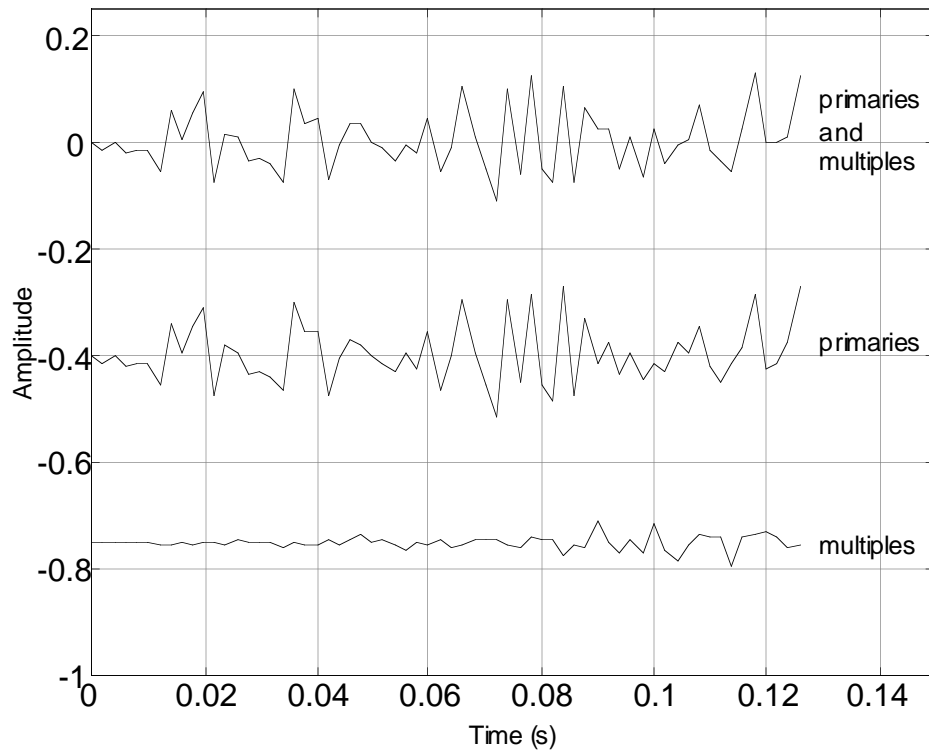


(b) Multiples

Fig. 11. Comparisons with difference plots for the constant velocity random model.

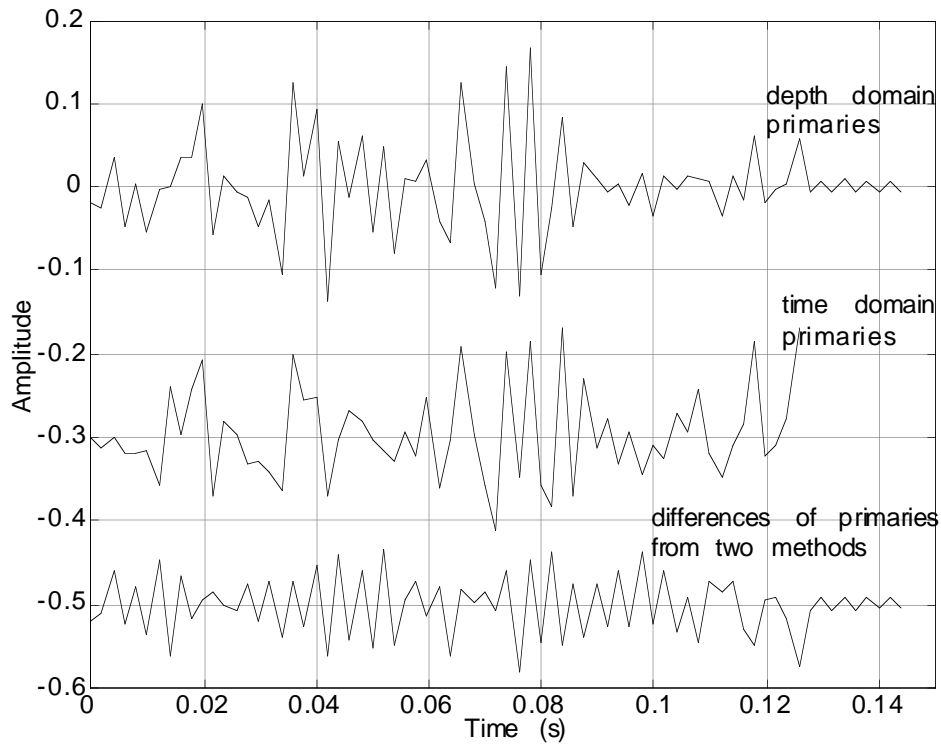


(a) Depth domain method

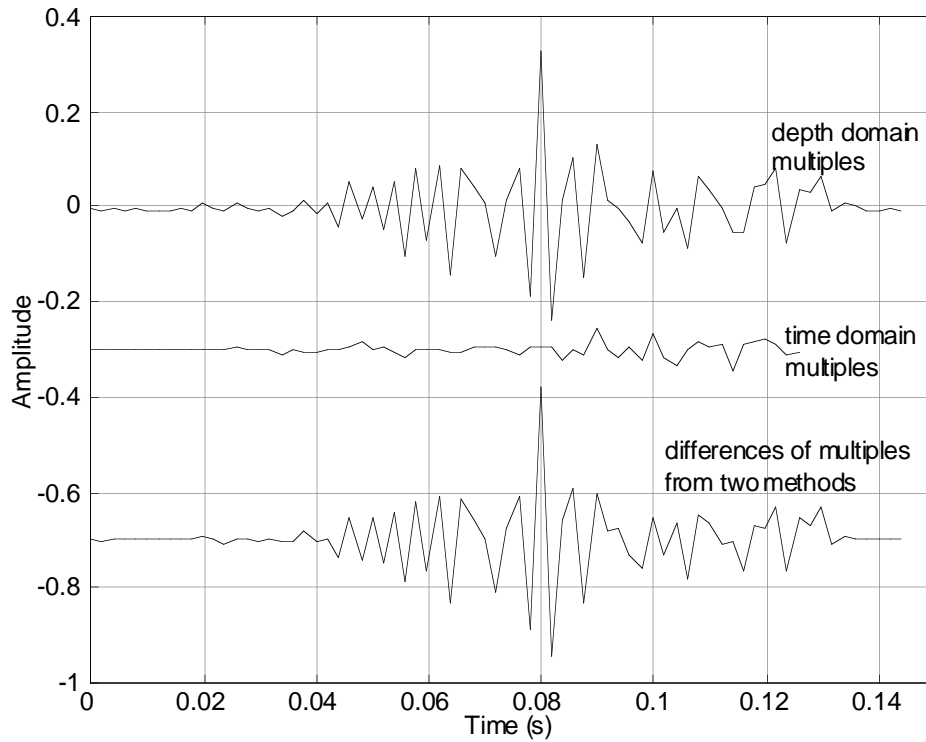


(b) Time domain method

Fig. 12. Responses of the two methods for the Blackfoot 08-08 well log data

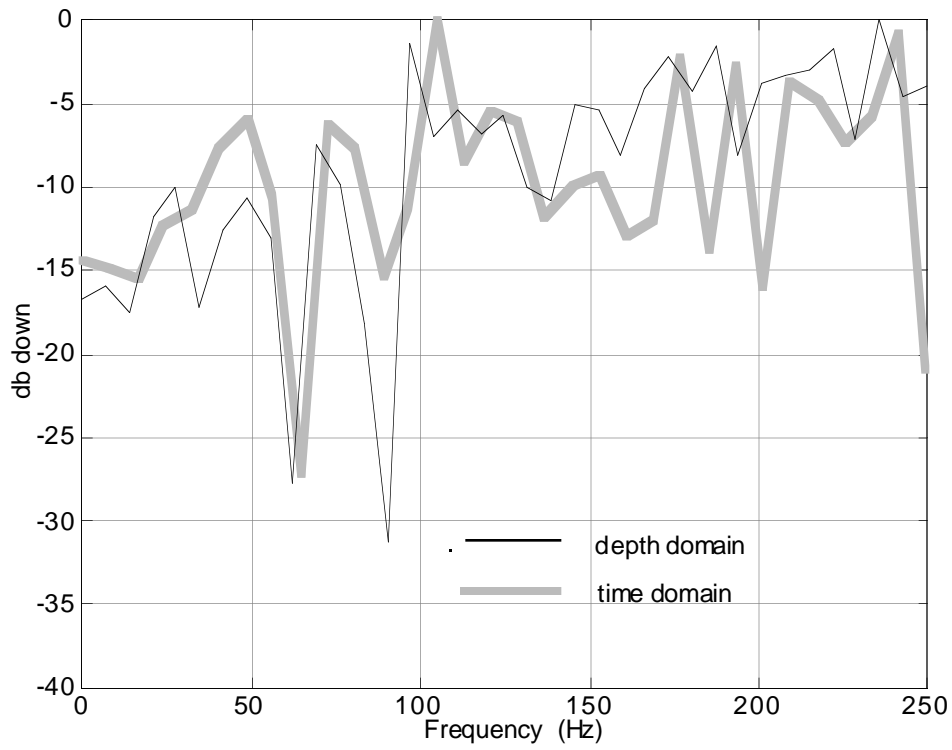


(a) Primaries

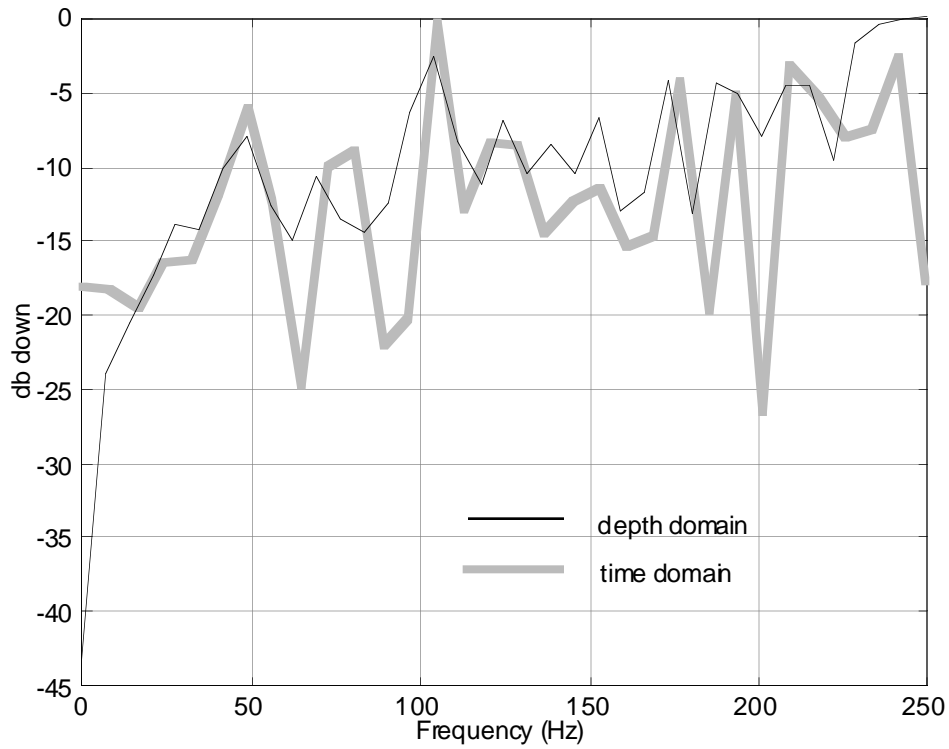


(b) Multiples

Fig. 13. Comparisons with difference plots for Blackfoot 08-08.



(a) Primaries with multiples



(b) Primaries only

Fig. 14. Amplitude spectra of primaries with multiples and primaries only from Blackfoot 08-08

From Figures 8 and 10, the relatively more chaotic nature of the multiples from the constant density model is again apparent. Comparisons of primaries and multiples between the two methods are given in Figure 9 for constant density and in Figure 10 for constant velocity. All of the responses have large positive and negative amplitudes. In the constant density case, the differences of primaries between the two algorithms tend to come from the large reflection coefficient interfaces (Figure 9(a)). The two algorithms are more divergent for the random model than for the step model (compare Figures 9 and 5). As expected, the overall power of the multiples is much larger for the random model than for the step model. The multiples often exceed primaries in amplitude so that they reinforce, cancel out or even dominate.

Our greatest interest is with the real Blackfoot 08-08 logs, for which the responses of the time domain and depth domain techniques are given in Figure 12. Unlike the synthetic examples, these are shown without a wavelet because the logs are very short and a normal wavelet removes most of the detail. The results of the two methods are surprisingly different, even for the primaries (Figures 12 and 13). The time domain method creates primaries with less amplitude range and much smoother multiples than the depth domain method does. These are due to the small depth interval for these logs (0.3m) and the rapid fluctuations of acoustic impedance (Figure 3). The time domain algorithm, whose time thickness (2ms) is now much larger than the true depth thickness, strongly averages the log properties. Thus the very important detail of the logs is altered. Theoretically, if we sample the logs finely enough in time, we should get the same result as from the depth domain. It seems also likely that the differences between the two algorithms will be increasingly important for high resolution data. This will be a subject for future investigation. The results from the depth domain algorithm show higher amplitude primaries and severe multiples. The multiples are small in the early part but accumulate rapidly from .04s reaching the highest peak at .08s due to interbed multiples from the coals

The other very interesting result from these synthetics are the spectral notches, in primaries plus multiples traces from both methods (Figure 14). Coulombe and Bird (1996) recently showed that interbed multiples created by the Mannville coals cause a notch at 50-70Hz in the spectra of real data. Also, by a formula given by O'Doherty and Anstey (1971), the calculated amplitude spectrum shows significant notches between 55- 110Hz. There is good qualitative agreement between these and our results. The coals occur in Blackfoot 08-08 at about 1500-1750m (Figure 3) and there are two notches at 60Hz and 90Hz in our amplitude spectra of primaries plus multiples (Figure 14). Though the time domain algorithm shows similar effects they are again different detail. We will investigate the interpretability of both methods in the future.

CONCLUSION

The depth domain algorithm or 1D acoustic modeling with phase shift extrapolation in depth, works well and gives qualitatively correct results for every synthetic model and also for the real data from Blackfoot 08-08.

The time domain algorithm works well with every synthetic model too and produces results similar to the depth domain method. For constant velocity the two methods are exactly equivalent. However, in the more realistic variable velocity setting they can give quite different results. For real log data, the time domain method requires an extra small time interval to maintain all of the original information. From our results, at a normal sample rate (2ms), the time domain method created notably different primaries compared to our depth domain method. This is a direct consequence of the time averaging. However they have an acceptable correlation for many purposes. On the

other hand, the multiple solution created from the same logs by the two methods are very different.

Our results support the conclusion of Coulombe and Bird (1996) that a series of coal beds causes notches in the amplitude spectrum of the seismograms. It seems quite likely that interbed multiples cause (or at least accentuate) these notches.

REFERENCES

- Aki, K. and Richards, P.G., 1980, *Quantitative Seismology, Theory and Methods*, W.H. Freeman and Company.
- Berryman, L.H., Goupillaud, P.L. and Waters, K.H., 1958, Reflections from multiple transition layers, part I-theoretical results : *Geophysics*, 23, 244-252.
- Coulombe, C.A., and Bird, N.D., 1996, Transition filtering by high-amplitude reflection coefficients: Theory, practice and processing considerations: *The Leading Edge*, 15, 1037-1042.
- Dankbaar, J.W.M., 1985, Separation of P and S waves: *Geophysical Prospecting*, 33, 970-986.
- Easley, D.T. and Foltinek, D.S., 1993, Synthetic seismogram for P and S waves using the Goupillaud model: 1993 Annual Research Report of The CREWES Project.
- Frasier, C.W., 1980, A new time domain reflection seismogram, Presented at 12th Offshore Technology Conference in Houston, Tex., May 5-8.
- Fuchs, K. and Müller, G., Computation of Synthetic seismograms with the reflectivity method and comparison with observations: *Geophys. J.R. astr. Soc.*, 23, 417-433.
- Gazdag, J., 1978, Wave-equation migration by phase shift: *Geophysics*, 43, 1342-1351.
- Kelly, K.R., Ward, R.W., Treitel, S., and Alford, R.M., 1976, Synthetic seismograms: A finite-difference approach : *Geophysics*, 41, 2-27.
- Kennett, B.L.N., 1980, Seismic waves in a stratified half space-II. theoretical seismograms: *Geophys. J.R. astr. Soc.*, 61, 1-10.
- Lawton, D.C., and Howell, T.C., 1992, P-P and P-SV synthetic stacks, Expanded Abstract, 62nd SEG Annual International Meeting, October 25-29, New Orleans, USA, 1344-1347.
- Margrave, G.F. and Foltinek, D.S., 1995, Synthetic P-P and P-SV cross sections: 1995 Annual Research Report of The CREWES Project.
- Stephen, R.A., 1983, A comparison of finite difference and reflectivity seismograms for marine models: *Geophys. J.R. astr. Soc.*, 72, 29-57.
- Waters, K.H., 1992, *Reflection Seismology : A tool for energy resource exploration*, 3rd edition, Krieger Publishing Co.